

Visible light active Ag, N co-doped titania in the photo-oxidation of some 9-(*N,N*-dimethylaminomethyl)anthracene systems

K. M. Mothi · G. Soumya · A. H. Salim ·
S. Sugunan

Received: 18 November 2013 / Accepted: 2 May 2014 / Published online: 1 June 2014
© Springer Science+Business Media New York 2014

Abstract Irradiated semiconductor catalysis in the presence of molecular oxygen can be admitted as an innovative and economical process for the conversion of harmful aromatics to less harmful products. The present work reports the preparation of a co-doped system by sonication assisted sol–gel technique followed by calcination at 500 °C and checks its activity in photo-oxidation reactions. The prepared system was characterized by various physico-chemical techniques such as X-ray diffraction, Raman spectroscopy, IR spectroscopy, TG-DTG, UV-DRS, SEM, and XPS. Thermal stability and structural identity were observed from TG and XRD measurements respectively. On reaction, Tertiary amine appended anthracene and its phenyl substituted derivative in CH₃CN yielded Anthraquinone as the major product. Substituted Anthracenemethanamine reacted slowly and a relatively stable intermediate could be isolated at shorter periods of time. The products were separated and purified by column chromatography and the resultant products were characterized thoroughly by ¹H NMR, IR spectroscopy and GCMS analysis.

Keywords Ag–N–TiO₂ · Co-doping · Photo-oxidation · Anthraquinone · Anthracenemethanamine

1 Introduction

Heterogeneous semiconductor photocatalysis has recently got immense significance due to its heavy application in environmental pollution control [1]. Among various semiconductor materials, titania paves more attention due to its stability, non-toxicity, environmental tolerance, low cost and better catalytic activity [2]. TiO₂ crystallizes in three allotropic forms namely anatase, rutile and brookite out of which anatase is considered photocatalytically more active. Due to its large band gap (3.2 eV), the spectral response is limited in the UV region which constitutes only 4–5 % of the sun light. Band gap narrowing is an effective way to shift the spectral response of TiO₂ and could be attained by anion doping [3–5]. Doping of TiO₂ by metals such as Pt, Ag, Au, Cu, Ni and Pd prevent the electron–hole (e[−]–h⁺) recombination, resulting in an improved catalytic efficiency [6–8]. The above mentioned modifications however reduce the oxidative power and stability of the system concerned. The drawbacks of titania systems could be removed by another efficient method known as co-doping using Pd and N, V and N etc., where one element shifts the spectral response while the other lowers the electron–hole recombination [9–11]. Theoretical investigations revealed that the carrier lifetime in co-doped systems is longer than that in systems with single dopant [11].

Polycyclic aromatic hydrocarbons (PAH) are found naturally and also formed by the incomplete combustion of oil, garbage etc. These are one of the structural constituents of dyes, plastics, and pesticides. Effluents from coir and textile industries contain anthracene based PAH which results in the contamination of drinking water. Due to the presence of stable benzene rings, most of the PAH show strong inhibition towards biological degradation and the common methods employed for their removal [12]. According to

K. M. Mothi · G. Soumya · S. Sugunan (✉)
Department of Applied Chemistry, Cochin University of Science
and Technology, Cochin 22, Kerala, India
e-mail: ssg@cusat.ac.in

A. H. Salim
Department of Physics, College of Science, Sultanate of Oman,
36, Muscat, Oman

environmental protection agency, most of the PAH are highly toxic in nature. TiO_2 photochemistry has been extensively investigated as a method for the catalytic conversion of such organic compounds [13], highlighting the potential of thereof in the green chemistry. Photocatalysis is also used in organic synthesis, as it eliminates the use of many toxic chemicals and reduces the number of steps in the reaction. Electronically excited states of irradiated photocatalyst induce electron or energy transfer reactions and needs only milder reaction conditions. Also, the possibility of undesirable side reactions could be eliminated. Here we report the preparation of Ag, N co-doped TiO_2 catalytic system via sol–gel technique and its characterization. The catalytic activity of the prepared system was checked in the photo-oxidation of Anthracenemethanamines. By using our system, we were able to convert these to Anthraquinone (AQ), a compound having lesser toxicity than that of the starting compounds. Photocatalysis by Ag–N– TiO_2 is very rare and to the best of our knowledge, we are the first to report an organic transformation based on this co-doped system. Here we have used Ag(1 wt%)–N– TiO_2 system for entire photo-oxidation reactions. High visible light response of Ag and N co-doped TiO_2 system has been reported elsewhere.

2 Experimental methods

2.1 Materials and methods

Titanium(IV) isopropoxide, Silver nitrate and Urea were used as obtained from Sigma Aldrich, Germany. All the solvents were purchased from Merck Pvt. Ltd. India. The substrates used for photo reaction was synthesized in the organic chemistry laboratory of, Department of Applied Chemistry, CUSAT. Structure, crystalline nature, phase purity, lattice parameters and impurity defects of the catalyst was identified by X-ray diffraction analysis. Crystallite size of the sample was calculated by Scherrer's formula. The powder X-ray diffraction of the sample was performed using a Bruker AXS D8 diffractometer with Ni filtered Cu $K\alpha$ radiation source ($\lambda = 1.5406 \text{ \AA}$) in the range of $10\text{--}70^\circ$ at a scan rate of $0.5^\circ/\text{min}$. Thermal stability, decomposition temperature, phase change etc. were identified by thermal analysis. Thermal analysis were done using a Perkin Elmer Pyris Diamond thermo gravimetric/differential thermal analyzer under nitrogen atmosphere at a heating rate of $10^\circ\text{C}/\text{min}$ from room temperature to 800°C , where the samples were mounted on a platinum sample holder. Light response of the catalysts were recorded in the range of $200\text{--}900 \text{ nm}$ on Labomed UV–Vis double beam UVD-500 spectrophotometer with a CCD detector, using BaSO_4 as reflectance standard. SEM was used to understand the morphology of the sample. Compositional analysis was analyzed by EDX using JEOL Model JED-2300.

SEM micrographs were taken using JEOL Model JSM-6390LV with a resolution of 1.38 eV . For the supporting evidence, we have carried out Raman spectra measurements using a micro Raman system from Jobin–Yvon Horibra LABRAM-HR with a He–Ne Laser Source (633 nm) and Argon (488 nm). Functional groups and titania based stretching vibrations were observed from Thermo NICOLET FT-IR instrument. Surface composition and electronic structures were analyzed by X-ray photoelectron spectroscopy using an Omicron Nanotechnology XPS system with a monochromatic Al $K\alpha$ radiation ($h\nu = 1,486.6 \text{ eV}$) of source voltage 15 kV and emission current of 20 mA . All scans were carried out at ultrahigh vacuum of $2 \times 10^{-10} \text{ mbar}$. The obtained XPS spectra were de convoluted using Casa XPS program, (Casa Software Ltd, UK), in which the background was simulated using the Shirley function and the peaks were fitted using a Gaussian–Lorentzian function. All binding energies were referenced to C1s for calibration. Mass data of the products were analyzed by GCMS analyzer equipped with 5975C inert MSD with Triple-Axis Detector and 7890A GC system.

2.2 Preparation of the catalyst

Ag–N– TiO_2 system was prepared by sonication assisted sol–gel technique. 10 ml of $\text{Ti}[\text{OCH}(\text{CH}_3)_2]_4$ was dissolved in 30 ml of ethanol by vigorous stirring at room temperature, and called as first solution. Desired amount of $\text{Ag}(\text{NO}_3)_2$ and urea (urea to $\text{Ti}[\text{OCH}(\text{CH}_3)_2]_4$ was taken in a 1:1 molar ratio) were dissolved in 1:1 volume mixture of ethanol/acetic acid and called as the second solution. Both solutions were mixed together and sonicated for about 3 h in order to carry out hydrolysis. After proper ageing, the obtained Gel was dried at 100°C and calcined at 500°C for 4 h . The catalyst thus obtained was designated as Ag(1 wt%)–N–Ti.

2.3 Preparation of reactants

9-(*N,N*-dimethylaminomethyl)anthracene was synthesized using Leuckart reaction [14]. The description of the preparation procedure is as follows. To a solution of 9-anthraldehyde (3.0 g) in 15 ml of dry DMF, formic acid (0.8 ml of 90% solution) was added and stirred under reflux for 12 h . Excess solvent was removed by distillation under reduced pressure and the residual oil dissolved in ether solution was filtered and concentrated. Purification of 9-(*N,N*-dimethylaminomethyl)anthracene was carried out by an alumina column using 9:1 hexane/dichloromethane mixture as the mobile phase. The preparation of phenyl protected derivative of 9-(*N,N*-dimethylaminomethyl)anthracene is an arduous process and consist of a series of reactions. 9-phenyl anthracene was synthesized using Grignard reaction. Here 1:1 equivalent of anthrone in dry THF was mixed with phenyl magnesium chloride and stirred properly in an ice cold condition. The

above reaction mixture was stored at 5 °C for 12 h and then added NH_4Cl and excess ether. After that the concentrated mixture was acidified using con. HCl and the obtained white precipitate was extracted with DCM and washed with NaHCO_3 . Pure compound was obtained using silica column with hexane as the mobile phase. 9-phenyl-10-anthraldehyde was synthesized using Vilsmeier-Hack reaction. For this reaction, reflux a mixture of phenyl anthracene (0.8 g), *N*-methyl formamide (0.8 ml) and POCl_3 (0.8 ml) in ortho dichloro benzene for 7 h. Then the mixture was washed with sodium acetate solution followed by DCM extraction. The pure compound was separated by silica column using 80:20 hexane/DCM as the mobile phase. Finally the targeted compound, 10-phenyl-9-(*N,N*-dimethylaminomethyl)anthracene was prepared from 9-phenyl-10-anthraldehyde using the same procedure (Leuckart reaction) adopted for the synthesis of 9-(*N,N*-dimethylaminomethyl)anthracene.

2.4 Photocatalytic reaction

Photocatalytic reactions were carried out in an Oriel Arc lamp system designed to produce uniform illumination. The diameter of the collimated beam is around 1 inch (2.54 cm) and the work plane is 2.6 inches (6.65 cm) from the lower end of the beam tuning assembly. In order to control the temperature for the lamp environment, uniform illuminator was equipped with fan cooled lamp housing. The light source was either 100 or 150 W Xe ozone free lamps with average life of 1,500 h. A 420–630 nm dichroic mirror (cold mirror) filter was used in order to get visible radiation, which gave an irradiance of 64.7 mW/cm^2 (100 W) and 96.8 mW/cm^2 (150 W) respectively.

Photo-oxidation reactions were carried out as follows. 9-(*N,N*-dimethylaminomethyl)anthracene systems in CH_3CN (0.03 M) were taken in a 100 ml beaker and 0.1 g of the catalyst was added to it. The mixture was stirred for about 30 min to achieve an adsorption/desorption equilibrium before placing under the lamp setup. Then the suspension was irradiated for 3 h. As a control, we also carried out the same reaction without the catalyst. The resultant mixture was centrifuged and filtered using a Whatman filter paper. This was further purified by silica column chromatography using 70:30 hexane/DCM mixtures as the mobile phase. Isolated products were thoroughly characterized using various techniques such as melting point, FT-IR, ^1H NMR, and GCMS analysis.

3 Results and discussion

3.1 X-ray diffraction

X-ray diffraction is a powerful and nondestructive technique used to understand the crystallographic phases present in a

sample. Figure 1 shows the XRD pattern of $\text{Ag}(1 \text{ wt}\%)\text{-N-Ti}$ calcined at 500 °C for 4 h. It is clear from the spectrum that photocatalytically active anatase phase dominates in the calcined samples, with peaks at 2θ values around 25.4°, 38°, 48.1°, 55.2° and 62.7° corresponding to (101), (004), (200), (211) and (204) crystal planes (JCPDS 21-1272), respectively [15]. There are no characteristic peaks corresponding to dopants, which may be due to their low concentration. Crystallite size is a measure of the size of a coherently diffracting domain. Crystallite size of the sample was calculated from Scherrer's equation by using full width at half maximum of the (101) peak of the anatase phase. Crystallite size of pure TiO_2 and co-doped system were found to be 18.2 and 15 nm respectively. Doping of low concentration of impurities has no noticeable effect on the crystallite size. But the crystallite size of $\text{Ag}(1 \text{ wt}\%)\text{-N-Ti}$ was found to be lower than that of bare TiO_2 , which indicates that the doping of Ag ions having higher ionic radius into the lattice of TiO_2 causes some lattice distortion, which suppress the growth of TiO_2 nanoparticles. Strain energy accumulated in the crystal due to the introduction of larger Ag ions also inhibits the phase transition from anatase to rutile. Sharp and intense peaks indicate the highly crystalline nature of the codoped system.

3.2 Raman spectroscopy

Raman spectroscopy is a sensitive technique employed to investigate the surface homogeneity and the nature of the crystallographic phases. Figure 2 shows the Raman spectra of the prepared samples. The structural identity of the prepared system obtained from XRD spectrum is further confirmed by Raman spectra measurements. Anatase has six Raman active modes. Well resolved Raman peaks at 143 cm^{-1} (E_{1g}), 197 cm^{-1} (E_{2g}), 399 cm^{-1} (B_{1g}), 540 cm^{-1} (combination of

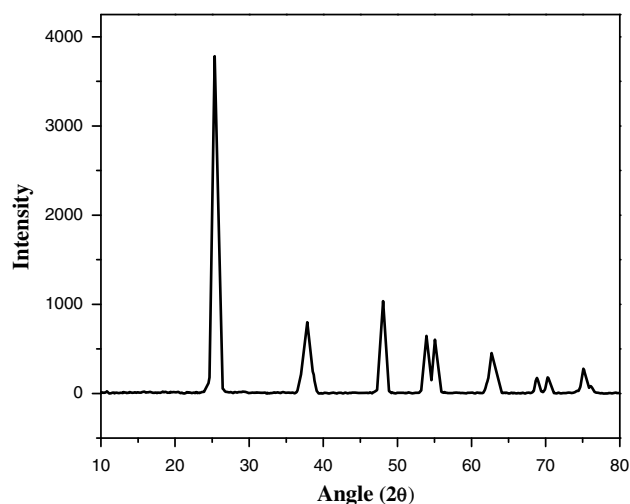


Fig. 1 XRD pattern of $\text{Ag}(1 \text{ wt}\%)\text{-N-Ti}$ system

A_{1g} and B_{1g}) and 639 cm^{-1} (E_g) in the spectra of calcined samples point to the presence of Anatase phase [16]. Absence of Raman peaks corresponding to Ag and N indicates the homogeneous structure of the prepared sample with less lattice distortion. The intensity of the lowest vibration peak at 145 cm^{-1} was found to be increased and its width broadened after the addition of dopants [17–19]. This suggests an enhanced crystallite property and a reduction in particle size.

3.3 FTIR analysis

Titania based stretching vibrations and functional groups were identified from IR spectroscopy results. The presence of water and O–H groups on the surface of the particles is supported by the presence of two strong bands at $3,430$ and $1,630\text{ cm}^{-1}$, which are attributed to the stretching and bending vibrations of O–H group respectively. A highly intense band around 590 cm^{-1} is due to the Ti–O and O–Ti–O vibrations of titania [20]. No absorption corresponding to the dopant species were observed.

3.4 Scanning electron microscopy

Surface morphology of the catalyst is evidenced from SEM image (Fig. 3). Knowledge of surface morphology helps in interpreting photocatalytic reactions. Catalyst morphology can sometimes affect the light absorption ability and generation of excitons, which in turn gets reflected in its efficiency. Preparation procedure and composition may change the surface morphology. The prepared sample (Fig. 3) consists of nearly spherical particles with some degree of aggregation. The shapeless structures in the image are mainly due to aggregation. However these aggregates cannot negatively influence the catalytic activity.

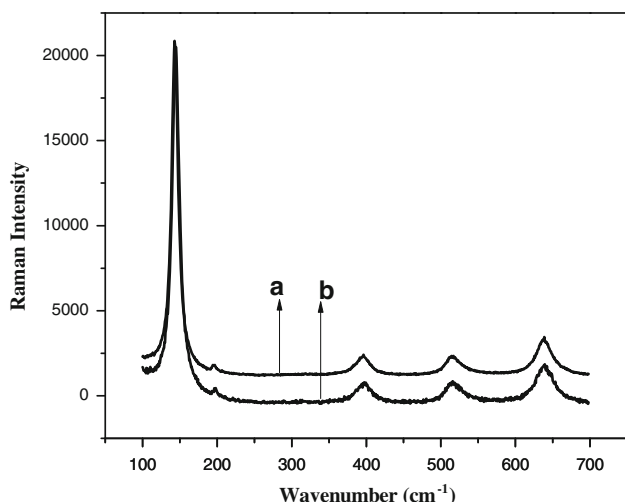


Fig. 2 Raman spectra of *a* Ag(1 wt%)-N-Ti. *b* TiO₂

3.5 UV–Vis Spectra

Figure 4 shows the UV–Vis reflectance spectra of pure TiO₂ and the co-doped system. Spectral response of pure TiO₂ is in the UV region, but the co-doping extends the spectral response to the visible region. The absorption edge energy of the co-doped system was calculated using the equation, $E_g = 1,240/\lambda$ [21]. This is one of the simple versions of Kubelka–Munk equation, where λ represents the wavelength from which reflection has taken place. The band gap of the co-doped system was calculated to be around 2.4 eV, which is lower than that of bare TiO₂ (3.2 eV). The lower band gap indicates the incorporation of dopants into the lattice of semiconductor material. Lower or nearly similar ionic radii of the dopants facilitate substitutional doping at cationic as well as anionic sites, which is responsible for the better reduction of the band gap.

3.6 Thermal analysis

Figure 5 represents the TG-DTG curves of Ag(1 wt%)-N-Ti system. Thermo gravimetric analysis (TGA) was carried out to study the thermal decomposition process of the precursor and stability of the prepared system. This also gives information regarding phase change, hydration etc. Mass changes occur in a variety of ways and this produces steps in TGA or peaks in the differential thermo gravimetric (DTG) curve (Fig. 5). A weight loss in the range of $76\text{--}110\text{ }^\circ\text{C}$ is assigned to the loss of adsorbed water. Another weight loss in the range of $144\text{--}190\text{ }^\circ\text{C}$ represents the initial decomposition of urea. A very sharp and narrow weight loss located around $244\text{--}320\text{ }^\circ\text{C}$ indicates the complete decomposition of silver nitrate and urea. After $400\text{ }^\circ\text{C}$, there is no noticeable weight loss on TG, which indicates the stability of the catalyst and hence the calcination temperature was fixed at $500\text{ }^\circ\text{C}$.

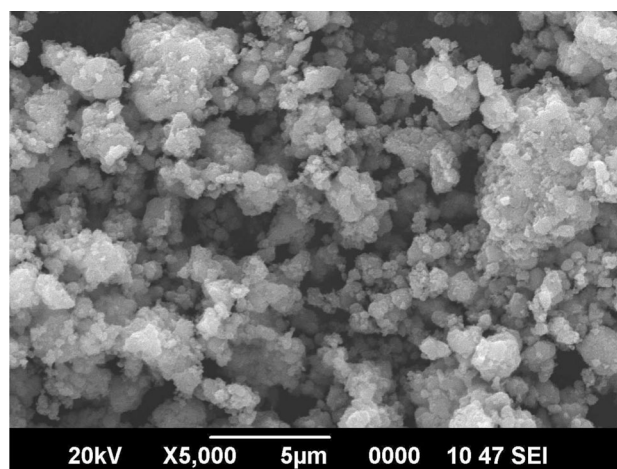


Fig. 3 SEM image of Ag(1 wt%)-N-Ti system

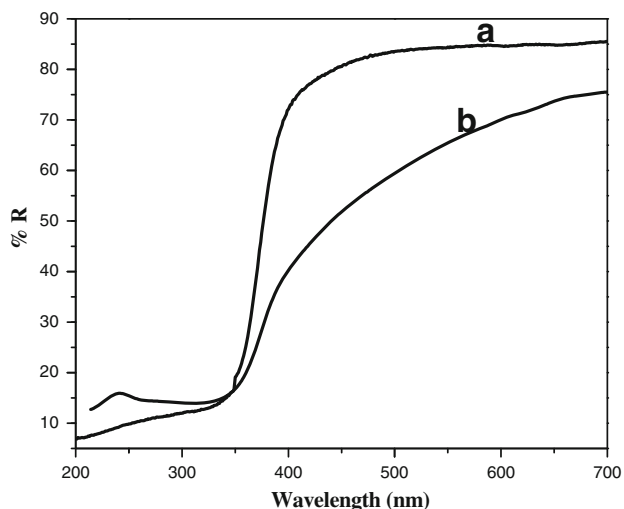


Fig. 4 UV-DRS spectra of *a* TiO₂, *b* Ag(1 wt%)-N-Ti

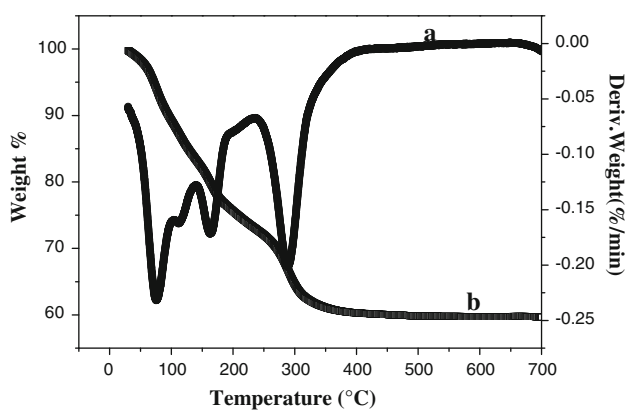


Fig. 5 *a* DTG and *b* TG curves of Ag(1 wt%)-N-Ti

3.7 XPS analysis

Chemical composition and surface states of elements in the co-doped system were identified by XPS analysis. Binding energy corresponding to Ti2p, Ag3d, N1s and O1s core levels can be seen from the survey scan of co-doped system (Fig. 6). In pure TiO₂, Ti2p_{3/2} and Ti2p_{1/2} core levels can be observed at binding energies 456 and 464 eV with an energy difference of 8 eV confirming the presence of Ti⁴⁺ species. But the co-doped TiO₂ shows Ti2p_{3/2} and Ti2p_{1/2} core levels at 459 and 464.8 eV respectively (Fig. 7). The shift of these Ti 2p peaks in co-doped TiO₂ suggests the difference in the electronic interaction of Ti with ions and a better incorporation of dopants into the lattice. The binding energies of Ag3d_{5/2} (368 eV) and Ag3d_{3/2} (374 eV) reveals that silver is in the form of AgO in the prepared system (Fig. 8). The signal at a binding energy of 399 eV (Fig. 9) is attributed to the O-Ti-N linkage in the system [22].

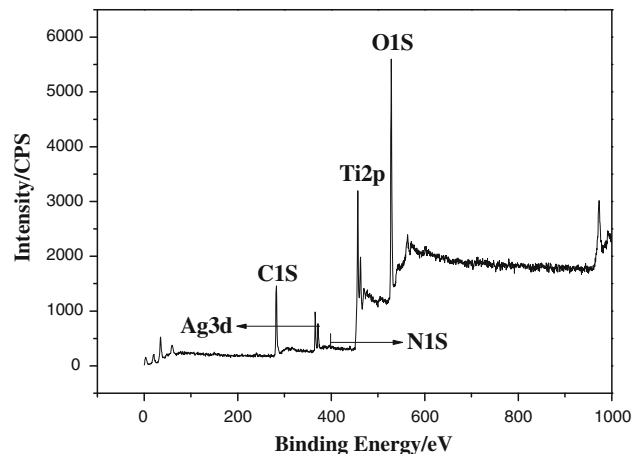


Fig. 6 XPS Survey scan of Ag(1 wt%)-N-Ti system

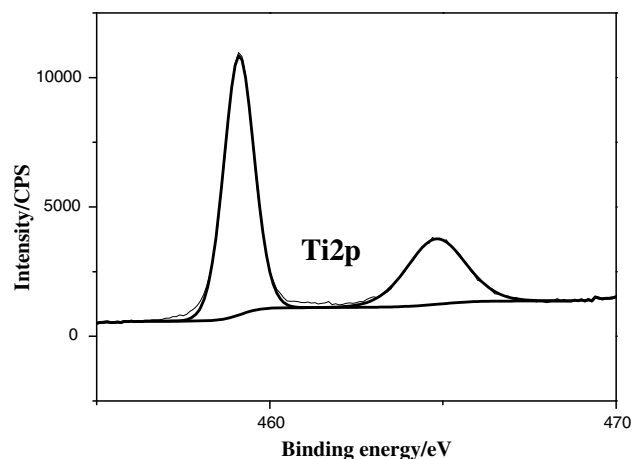


Fig. 7 High resolution XPS scan over Ti2p levels of Ag(1 wt%)-N-Ti system

Higher binding energy of nitrogen around 401.2 eV (Fig. 9) represents the presence of some surface nitrogen species [23]. The major O1s core level at 529 eV and a shoulder at 531 eV (Fig. 10) indicate the presence of lattice oxygen (Ti-O) and oxygen from surface hydroxyl groups respectively.

3.8 Catalytic activity studies

Catalytic activity of the prepared system was evaluated by monitoring the photo-oxidation of 9-(*N,N*-dimethylamino-methyl)anthracene and its phenyl protected derivative as described in Sect. 2.4. The spacer group (-CH₂) present in the substrate molecules effectively shuts down the communication between the donor and acceptor species and offer an easy method to study the photo induced electron transfer reaction. The anthracene derivatives used were not

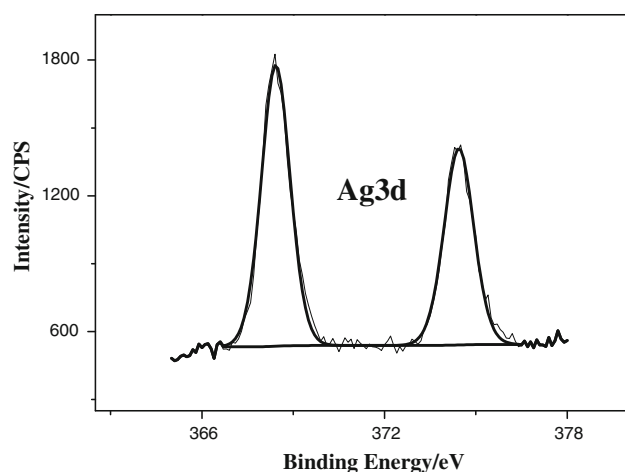


Fig. 8 High resolution XPS scan over $Ag3d$ core levels of $Ag(1\text{ wt}\%)-N-Ti$ system

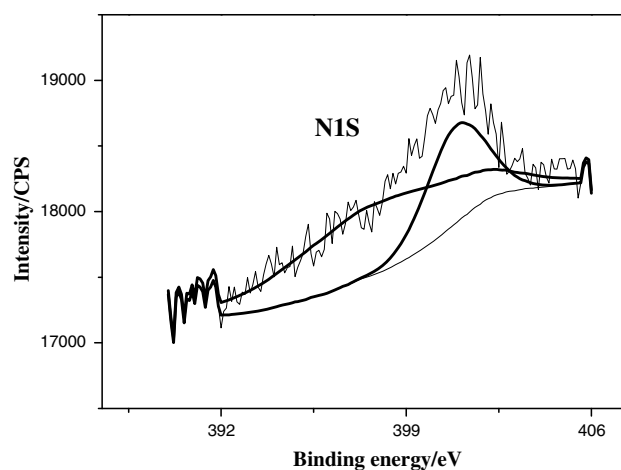


Fig. 9 High resolution XPS scan over $N1s$ level of $Ag(1\text{ wt}\%)-N-Ti$ system

active under visible light irradiation because their absorption maximum was found to be around 354 nm. So the possibility for sensitization of co-doped TiO_2 by anthracene derivative is marginal. Irradiation of the suspension using visible light results initial excitation from the co-doped catalyst, which drives the reaction effectively. That is, the intermediate species responsible for the generation of reactive oxygen species purely originated from the co-doped catalytic system.

Antraquinone was the only product obtained after photo-oxidation of 9-(*N,N*-dimethylaminomethyl)anthracene, with 82 % yield using 150 W lamp. Light and molecular oxygen are the two major driving forces in photo-oxidation reactions. In this reaction, molecular oxygen was not added to the reaction mixture externally. Upon irradiation with visible light, electrons in the valence band of the catalyst could get excited and get accumulated in the conduction band. These electrons could easily be captured by molecular oxygen adsorbed on the catalyst surface to form some reactive oxygen species, which in turn react with the substrate molecules. Molecular oxygen not only acts as scavenger for electrons but is also responsible for producing some reactive species.

In the second case, 10th position of the 9-(*N,N*-dimethylaminomethyl)anthracene was protected by a phenyl ring. Surprisingly within the time limit of 3 h, an intermediate species, 9-hydroxy 9-phenyl anthrone (9H9PA) could be obtained in good yield (150 W). When the reaction time was increased to 4 h, AQ was obtained as the major product (84 %, 150 W) (Fig. 11). The phenyl ring at the 10th position reduces the feasibility of photo-oxidation reaction and the stability of the intermediate compound allows its easy identification and separation. Increasing the reaction time leads to extensive degradation,

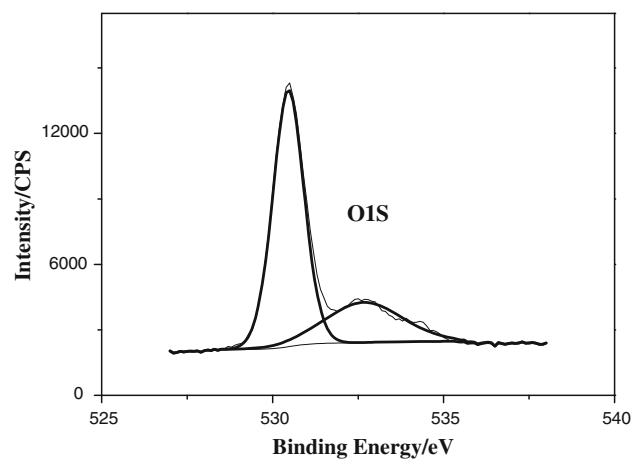


Fig. 10 High resolution XPS scan over $O1s$ level of $Ag(1\text{ wt}\%)-N-Ti$ system

resulting in the loss of phenyl group to form AQ. The detailed reaction mechanism is shown in Fig. 12 and the results of photo-oxidation reactions are tabulated in the Table 1. Catalysts capable of inducing the oxofunctionalization of hydrocarbons using this environmentally benign and cheap reagent has got immense significance in synthetic and industrial points of view.

The amount of the catalyst was chosen to be 0.1 g since a lower amount (0.05 g) gave a marginal yield and a higher amount (0.15 g) made the suspension very thick for the light to transmit and resulted in a poor yield. As expected, the yield was higher with a lamp power of 150 W.

3.9 Analysis of photo-oxidation products

1H NMR spectrum of the AQ shows two doublet of doublets at δ -values in the range of 7.8–8.34 ppm indicating

Fig. 11 Possible way of interaction of reactive oxygen species with the substrate

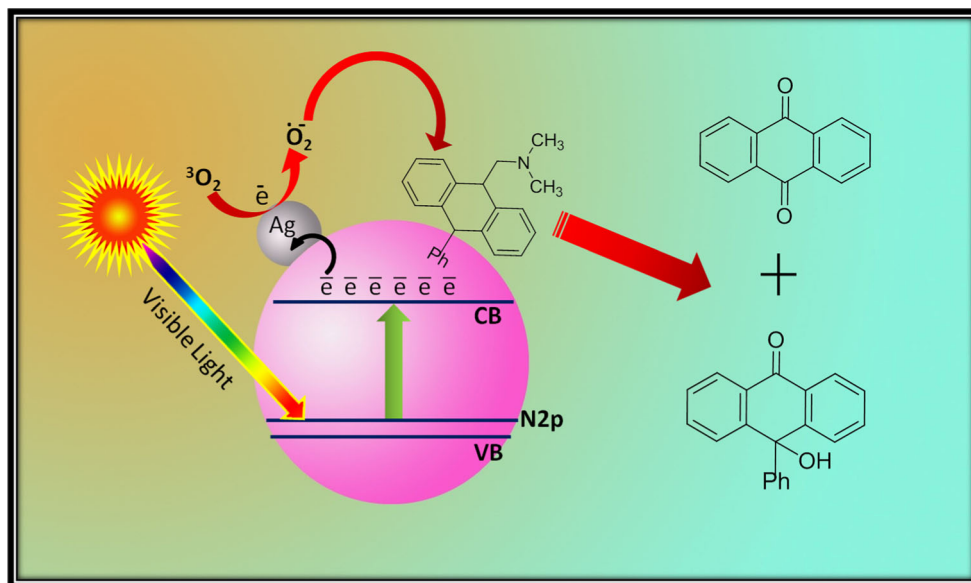


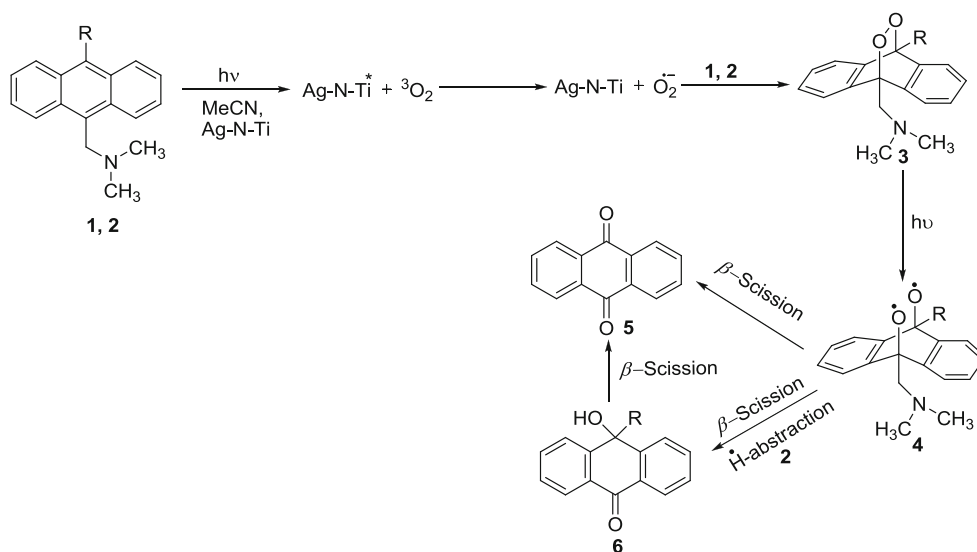
Table 1 Results of photo-oxidation reactions

Substrate	Time (h)	Products	Yield (%)
9-(<i>N,N</i> -dimethylaminomethyl)anthracene	3	AQ	82
10-phenyl-9-(<i>N,N</i> -dimethylaminomethyl)anthracene	3	9H9PA	70
10-phenyl-9-(<i>N,N</i> -dimethylaminomethyl)anthracene	4	AQ	12
10-phenyl-9-(<i>N,N</i> -dimethylaminomethyl)anthracene	4	AQ	84

Reaction conditions: concentration of the substrates: 0.03 M, catalyst amount: 0.1 g, solvent used: CH₃CN

two sets of four equivalent protons. GCMS spectrum shows *m/z* value at 208 corresponds to the *M*⁺ peak of AQ and it shows an *M*-28 peak at 180. FT-IR spectrum of AQ shows a strong band around 1670 cm⁻¹ corresponding to C=O stretching vibration and another band at 896 cm⁻¹ represents the stretching of substituted benzene ring. Proton NMR spectrum of 9-hydroxy 9-phenyl anthrone (9H9PA) shows multiplets having δ -values around 7.07–7.75 ppm representing the 13 aromatic protons. 9H9PA shows *M*⁺ peak at *m/z* 286 and *M*-77 peak at 209. FT-IR spectrum shows two strong bands at 3416 and 1600 cm⁻¹ corresponding to the O–H stretching and bending vibrations

Fig. 12 Detailed mechanism of photo-oxidation reaction



When R = H, compound 1 yielded only 5
When R = Ph, compound 2 yielded 5 and 6

respectively. Another prominent peak at 2922 cm^{-1} corresponds to C–H stretching vibration.

4 Conclusion

Semiconductor catalysis is an effective and greener way for the removal of environmentally harmful substances. Cost effective, recyclable, and environmentally benign; Ag/N co-doped TiO_2 system was prepared successfully by sonication assisted sol–gel method and characterized using various physico-chemical techniques. XPS measurements suggested a better distribution of the dopants and the visible light response was observed from the UV-DRS data. Ag/N co-doped TiO_2 was found to be highly active for the photo conversion of novel 9-(*N,N*-dimethylaminomethyl)anthracene and its phenyl substituted derivative into AQ, a compound having diverse applications in industrial as well as medical fields. The reaction components and the resultant products were characterized by various techniques such as ^1H NMR, Infrared spectroscopy and GCMS analysis.

Acknowledgments MKM is indebted to UGC-BSR for the fellowship. Help received from Dr. S. Prathapan (Associate Professor) and Jomon P. Jacob (SRF), Dept. of Applied Chemistry, CUSAT during photooxidation reaction and STIC, CUSAT for characterization is well acknowledged.

References

1. Kuvarega AT, Krause RWM, Mamba BB (2011) *J Phys Chem C* 115:22110–22120
2. Lin YM, Tseng YH, Huang JH, Chao CC, Chen CC, Wang I (2006) *Environ Sci Technol* 40:1616–1621
3. Zhao J, Chen C, Ma W (2005) *Top Catal* 35:269–278
4. Anpo MJ (2003) *Catal* 216:233
5. Asahi R, Morikawa T, Ohwaki T, Aoki K, Taga Y (2001) *Science* 293:269–271
6. Brezova V, Blazkova A, Karpinsky L, Groskova J, Havlinova B, Jorik V, Ceppan M (1997) *J Photochem Photobiol A Chem* 109:177–183
7. Ikeda S, Sugiyama N, Pal B, Marci G, Palmisano L, Noguchi H, Uosaki K, Ohtani B (2001) *Phys Chem Chem Phys* 3:267–273
8. Fuente A, Hernandez-Alonso MD, Maira AJ, Martinez-Arias A, Fernandez-Garcia M, Conesa JC, Soria J (2001) *Chem Commun* 2718–2719
9. Kuvarega AT, Krause RWM, Mamba BB (2011) *J Phys Chem C* 115:22110–22120
10. Liu J, Han R, Zhao Y, Wang H, Lu W, Yu T, Zhang Y (2011) *J Phys Chem C* 115:4507–4515
11. Sun X, Liu H, Dong J, Wei J, Zhang Y (2010) *Catal Lett* 135:219–225
12. Shi Z, Yao S, Sui C (2011) *Catal Sci Technol* 1:817–822
13. Panayotov DA, Burrows SP, Morris JR (2012) *J Phys Chem C* 116:6623–6635
14. Vadakkan JJ, Mallia RR, Prathapan S, Rath NP, Unnikrishnan PA (2005) *Tetrahedron Lett* 46:5919–5922
15. Song S, Tu JJ, He ZQ, Hong FY, Liu WP, Chen JM (2010) *Appl Catal A* 378:169–174
16. Golubovic A, Scepanovic M, Kremenovic A, Askrabic S, Berec V, Dohcevic-Mitrovic Z, Popovic ZV (2009) *J Sol-Gel Sci Technol* 49:311–319
17. Ying W, Yan W, Yanling M, Hanming D, Yougkui S, Xian Z, Xiaozhen T (2008) *J Phys Chem C* 112:6620–6626
18. Shu Y, Yohei A, Masakazu K, Jinshu W, Qing T, Tsugio S (2005) *J Mater Chem* 15:674–682
19. Ye C, Jinlong Z, Feng C, Masakazu A (2007) *J Phys Chem C* 111:6976–6982
20. Liu J, Rong H, Zhao Y, Wang H, Lu W, Yu T, Zhang Y (2011) *J Phys Chem C* 115:4507–4515
21. Kubelka P, Munk F (1931) *Tech Phys* 12:593
22. Choi H, Antoniou MG, Pelaez M, De la Cruz AA, Shoemaker JA, Dionysiou DD (2007) *Environ Sci Technol* 41:7530–7535
23. Sakthivel S, Kish H (2003) *Chem Phys Chem* 4:487–490